nature geoscience

Article

https://doi.org/10.1038/s41561-023-01285-1

Increasing contribution of nighttime nitrogen chemistry to wintertime haze formation in Beijing observed during COVID-19 lockdowns

In the format provided by the authors and unedited

Table of Contents:

Evaluation of the vertical distribution of $p$$NO_3^-$ production using a 3-D model

One major aspect of the "inherent disconnect" concerns the representativeness of ground-based measurements to the entire boundary layer, which is a significant limitation of this research topic. Conducting measurements in the residual layer well above 300 m with heavy, sophisticated instruments such as the iodide CIMS is technically challenging. As far as we know, there are no such measurements in China. As suggested by the reviewer, we deployed a 3-D model (WRF-Chem) to explore this issue. This model has been previously used to evaluate the impact of COVID-19 lockdown on air pollution in East China[14], where all details of the modeling setup are illustrated. The vertical profiles of NO, NO_2, and O_3 concentrations, were scaled based on the ratio between modeled (28 m height) and measured concentrations before further analysis. The total heterogeneous loss rate of N_2O_5 is calculated as the difference between the total production rate of NO_3 and N_2O_5 and the loss of NO_3 to NO (see Eq. R1), with an assumption that the loss rate of N_2O_5 is γ-insensitive under high particle loadings[16]. Then the production rate of $p$$NO_3^-$ is calculated based on the yield of N_2O_5 as derived in our study (Eq. R2).

$$L(N_2O_5) = k1[NO_2][O_3] - k2[NO][NO_3]$$ (Eq. R1)

$$P(pNO_3^-) = (2 - \Phi)\, L(N_2O_5)$$ (Eq. R2)

Here, $k_1 = 1.4\times10^{-13}\exp(-2470/T)$, $k_2 = 1.8\times10^{-11}\exp(110/T)$, and $\phi = 0.45$.

Figure R2-5 displays the modeled vertical profiles of NO, NO_2, O_3 concentrations, and the calculated production rate of $p$$NO_3^-$ during severe haze episodes in both pre-lockdown and lockdown periods. The simulations indicate that while significant amounts of $p$$NO_3^-$ were formed in the residual layer (above ~500 m) in the pre-lockdown period, the formation was much more limited in the lockdown period due to low NO_2 concentration. This suggests that the contribution of the N_2O_5 pathway to $p$$NO_3^-$ may have been underestimated

during the pre-lockdown period but overestimated during the lockdown period. Nonetheless, the column-mean production rate of $p\mathrm{NO_3^-}$ during the lockdown period was estimated to be approximately three times larger than that in the pre-lockdown period, supporting our conclusion on enhanced nocturnal nitrogen chemistry. It is important to note that the accuracy of the 3-D modeling is not strictly validated with *in situ* observations, and thus all values shown in the figure should only be regarded as qualitative.

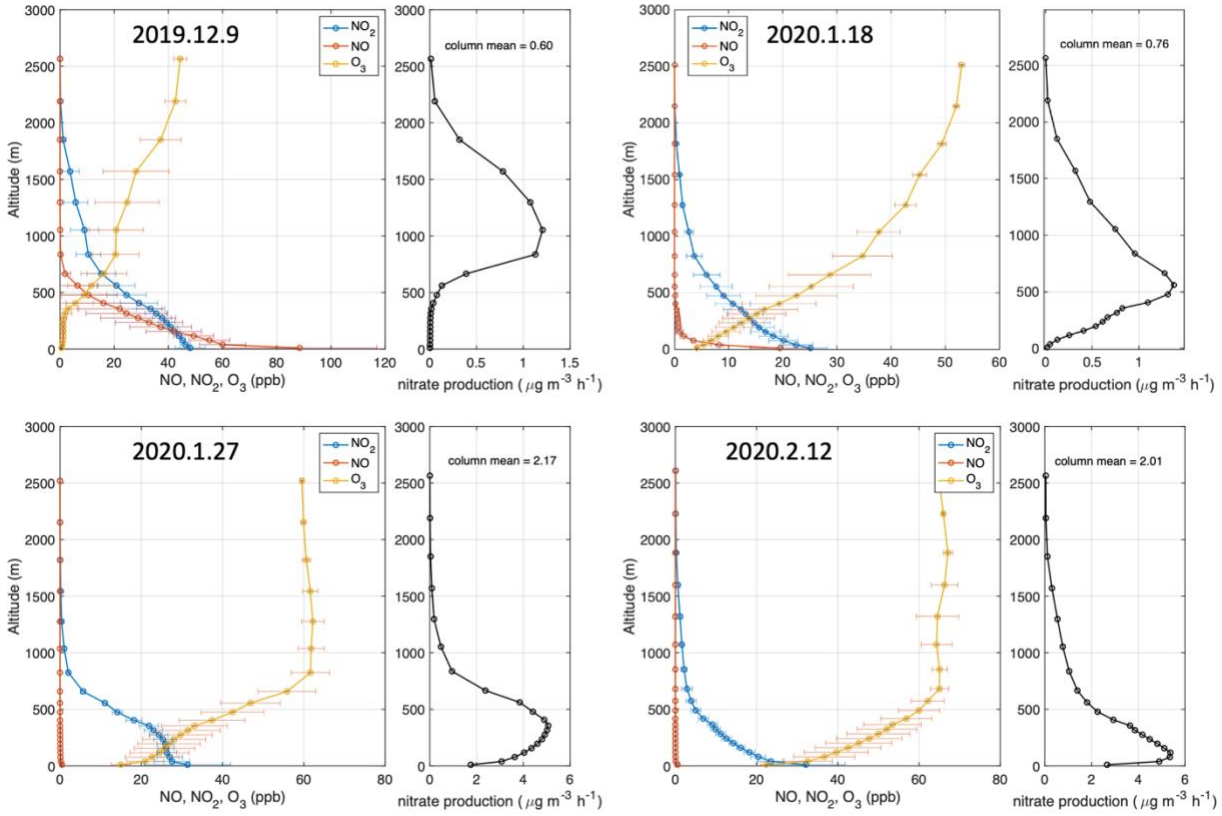

Figure S1. Simulated vertical profiles of NO, NO_2, and O_3 concentrations, as well as the calculated $p\mathrm{NO_3^-}$ production rate. The upper two panels are severe haze episodes in the pre-lockdown period, and the lower two panels are severe haze episodes in the lockdown periods. The error bar denotes the 1σ standard deviation of modeled concentration during the whole night. The relative error of the calculated $p\mathrm{NO_3^-}$ production rate is estimated to be less than $\pm$ 50 %.

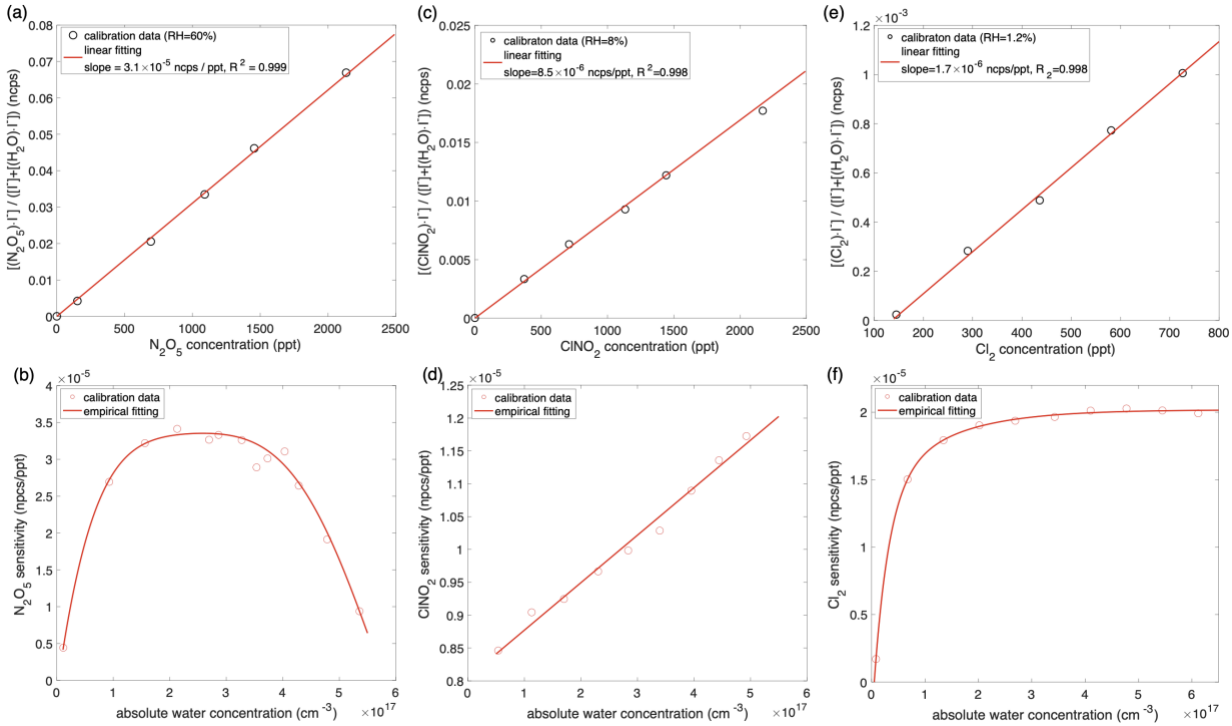

Fig. S2. Calibrations of N_2O_5, $ClNO_2$, and Cl_2, including multipoint calibrations at a constant RH (and constant water vapor concentration) (a, c, e) and calibrations of the sensitivity at varying concentrations of water vapors (b,d,f). Strong linearity can be seen in all calibration sets ($R^2 \geq 0.998$) for the multipoint calibration, and linear regression is used to derive the sensitivities. The dependence of sensitivities on water vapor concentration show different patterns, for which empirical fitting equations are used (red solid lines in Panels b, d, and f).

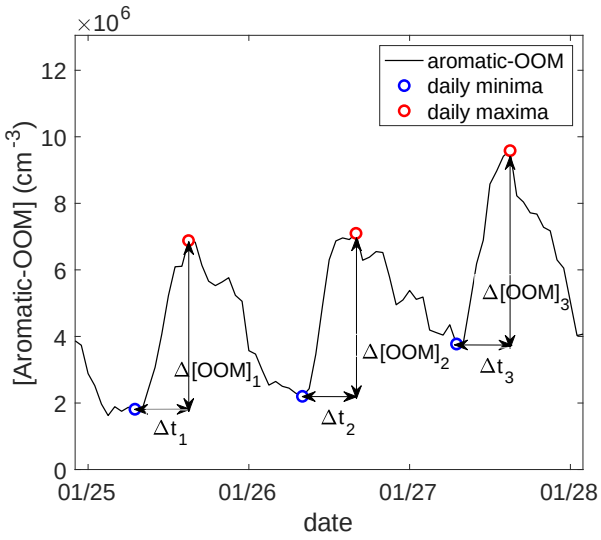

Fig. S3. Determination of Δ[aromatic-OOM] and its corresponding time window. Δ [aromatic-OOM]$_i$ is calculated on a daily basis as the difference between the minimum (blue circles) and maximum (red circles) of aromatic-OOM concentration; the corresponding time duration is defined as Δt_i.

Table S1. VOC and its reaction rate coefficient used for the calculation of VOC oxidation rate.

Formula	VOC	Adopted reaction rate coefficient, k (cm^3 $molecule^{-1}$ s^{-1})			
		with Cl	with OH	with NO_3	with O_3
C_6H_6	Benzene	1.30×10^{-15}	1.20×10^{-12}	1.10×10^{-17}	1.00×10^{-21}
C_7H_8	Toluene	6.20×10^{-11}	5.60×10^{-12}	2.01×10^{-17}	1.00×10^{-21}
C_8H_{10}	Ethylbenzene	1.15×10^{-10}	7.51×10^{-12}	5.71×10^{-16}	8.48×10^{-22}
C_9H_{12}	1,3,5-trimethylbenzene	1.94×10^{-10}	6.26×10^{-11}	8.00×10^{-16}	2.91×10^{-21}
$C_{10}H_{14}$	*p*-cymene	1.72×10^{-10}	4.85×10^{-12}	1.00×10^{-15}	5.00×10^{-20}
$C_{10}H_8$	Naphthalene	3.82×10^{-12}	3.69×10^{-11}	*n/a*	2.01×10^{-19}
C_4H_{10}	*n*-Butane	2.05×10^{-10}	2.30×10^{-12}	3.43×10^{-17}	1.00×10^{-23}
C_6H_{12}	Cyclohexane	2.01×10^{-10}	5.28×10^{-12}	1.35×10^{-16}	7.82×10^{-18}
C_4H_8	1-Butene	2.56×10^{-10}	3.48×10^{-11}	1.06×10^{-14}	6.72×10^{-18}
C_6H_{10}	Cyclohexene	3.49×10^{-10}	6.09×10^{-11}	6.58×10^{-13}	5.52×10^{-17}
C_5H_8	Isoprene	4.30×10^{-10}	1.00×10^{-10}	5.88×10^{-13}	7.20×10^{-18}

Note that *n/a* means the *k* for this reaction is not available.

Table S2. Details of the NO_x, O_3, $PM_{2.5}$, and CO measurements. The hourly data during wintertime were obtained from our measurements and open data sources.

	Site	Location	Site types	Data period
Europe	(a) Madrid, Spain	Escuelas Aguirre*	Urban	Feb, 2019
	(b) Berlin, Germany	Neukölln	Urban background	Dec, 2016, Jan, Feb, and Dec, 2017, Jan and Feb, 2018
	(c) Frankfurt, Germany	Schwanheim	Urban background	Dec, 2016, Jan, Feb, and Dec, 2017, Jan and Feb, 2018
	(d) Helsinki, Finland	Kumpula campus of University of Helsinki **	Urban	Jan, Feb, and Dec, 2019-2021, Jan and Feb, 2022
Asia	(e) Beijing, China	West campus of Beijing University of Chemical Technology	Urban	Jan, Feb, and Dec, 2019 Jan 1 – 22, 2020
	(f) Shanghai, China	Shanghai Academy of Environmental Sciences	Urban	Dec, 2019-2020, Jan and Dec, 2021, Jan, 2022
	(g) Nanjing, China	SORPES monitoring station	Suburban	Dec, 2020, Jan, 2021
	(h) Hong Kong, China	Tung Chung monitoring station	Suburban	Dec, 2021, Jan and Feb, 2022
	(i) Kolkata, India	Bidhannagar, Kolkata - WBPCB***	Urban	Nov-Dec, 2019
	(j) Delhi, India	CRRI Mathura Road, Delhi – IMD***	Urban	Nov-Dec, 2019
	(k) Jaipur, India	Adarsh Nagar, Jaipur - RSPCB***	Urban	Nov-Dec, 2019
North America	(l) Los Angeles, USA****	Pasadena-S Wilson Avenue****	Suburban	Nov-Dec, 2019
	(m) San Francisco, USA****	San Francisco-Arkansas Street****	Urban	Nov-Dec, 2019

Note: Websites of open data sources:
* https://datos.madrid.es/portal/site/egob;
** https://smear.avaa.csc.fi/ ;
*** https://app.cpcbccr.com/ccr/#/caaqm-dashboard-all/caaqm-landing;
**** https://www.arb.ca.gov/aqmis2/aqdselect.php?tab=specialrpt